Numerical simulations of shock acceleration in SNRs including magnetic field amplification

Vladimir Zirakashvili*, Vladimir Ptuskin*

**Pushkov Institute of Terrestrial Magnetism, Ionosphere and Radiowave Propagation, 142190, Troitsk, Moscow Region, Russia*

***Abstract*. A new numerical code describing the nonlinear diffusive shock acceleration is used for modeling of particle acceleration in supernova remnants. It contains coupled spherically symmetric hydrodynamic equations including forward and backward shocks and the transport equations for energetic particles. The effects of magnetic field amplification and MHD turbulence generation by cosmic ray streaming instability are included.**

***Keywords*: cosmic ray acceleration, supernova remnants**

I. Introduction

The diffusive shock acceleration process [12], [2], [3], [6] is considered as the principal mechanism for the production of galactic cosmic rays (CR) in supernova remnants (SNRs). The supernova (SN) material ejected during the explosion (SN ejecta) moves with a high supersonic velocity. The forward and backward shocks are formed due to ejecta interaction with a circumstellar medium. The circumstellar gas is compressed at the forward shock while the backward shock propagates into the supernova ejecta. The cosmic ray particles are accelerated at these shocks.

In this short report we present a new numerical model of the nonlinear diffusive shock acceleration [21]. This model is a natural development of existing models [5], [11]. The solution of spherically symmetric hydrodynamic equations is combined with the energetic particle transport and acceleration on the forward and backward shocks of a supernova remnant. Nonlinear response of energetic particles via their pressure gradient results in the self-regulation of acceleration efficiency.

II. Nonlinear model of diffusive shock acceleration

Hydrodynamical equations for the gas density $\rho(r,t)$, gas velocity $u(r,t)$, gas pressure $P_g(r,t)$, and the equation for isotropic part of the CR momentum distribution $N(r,t,p)$ in the spherically symmetrical case are given by

$$\frac{\partial \rho}{\partial t} = -\frac{1}{r^2}\frac{\partial}{\partial r} r^2 u \rho \qquad (1)$$

$$\frac{\partial u}{\partial t} = -u\frac{\partial u}{\partial r} - \frac{1}{\rho}\left(\frac{\partial P_g}{\partial r} + \frac{\partial P_c}{\partial r}\right) \qquad (2)$$

$$\frac{\partial P_g}{\partial t} = -u\frac{\partial P_g}{\partial r} - \frac{\gamma_g P_g}{r^2}\frac{\partial r^2 u}{\partial r} - (\gamma_g - 1)(w-u)\frac{\partial P_c}{\partial r} \qquad (3)$$

$$\frac{\partial N}{\partial t} = \frac{1}{r^2}\frac{\partial}{\partial r} r^2 D(p,r,t)\frac{\partial N}{\partial r} - w\frac{\partial N}{\partial r} + \frac{\partial N}{\partial p}\frac{p}{3r^2}\frac{\partial r^2 w}{\partial r}$$
$$+\frac{\eta_f \delta(p-p_f)}{4\pi p_f^2 m}\rho(R_f+0,t)(\dot{R}_f - u(R+0,t))\delta(r-R_f(t))$$
$$+\frac{\eta_b \delta(p-p_b)}{4\pi p_b^2 m}\rho(R_b-0,t)(u(R_b-0,t)-\dot{R}_b)\delta(r-R_b(t)) \qquad (4)$$

Here $P_c = 4\pi \int p^2 dp v p N/3$ is the CR pressure, $w(r,t)$ is the advective velocity of CRs, γ_g is the adiabatic index of the gas, and $D(r,t,p)$ is the CR diffusion coefficient. It was assumed that the diffusive streaming of CRs results in the generation of magnetohydrodynamic (MHD) waves. CR particles are scattered by these waves. That is why the CR advective velocity w may differ from the gas velocity u. Damping of these waves results in an additional gas heating. It is described by the last term in Eq. (3). Two last terms in Eq. (4) correspond to the injection of thermal protons with momenta $p = p_f$, $p = p_b$ and mass m at the fronts of the forward and backward shocks at $r = R_f(t)$ and $r = R_b(t)$ respectively. The dimensionless parameters η_f and η_b determine the injection efficiency.

We shall neglect the pressure of energetic electrons. In other words they are treated as the test particles. The evolution of electron distribution is described by equation similar to equation (4) with additional terms describing synchrotron and IC losses.

CR diffusion is determined by magnetic inhomogeneities. Strong streaming of accelerated particles changes medium properties in the shock vicinity. CR streaming instability results in the high level of MHD turbulence [3] and even in the amplification of magnetic field in young SNRs [4]. Due to this effect the maximum energy of accelerated particles may be higher in comparison with previous estimates of Lagage and Cesarsky [13].

According to the recent numerical modeling of this instability, the magnetic field is amplified by the flux of run-away highest energy particles in the relatively broad region upstream of the shock [20]. Magnetic energy density is a small fraction ($\sim 10^{-3}$) of the energy density of accelerated particles. This amplified almost

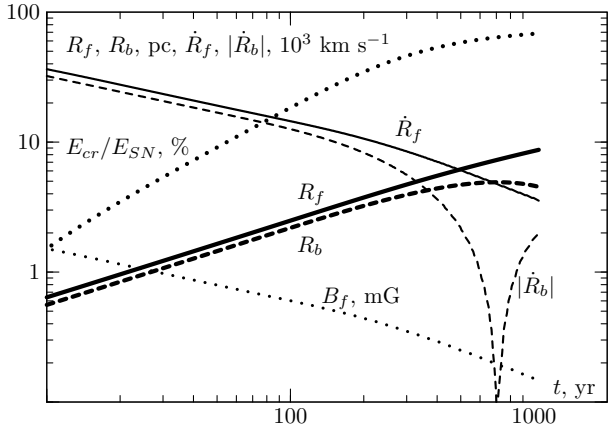

Fig. 1: Dependencies on time of the forward shock radius R_f (thick solid line), the backward shock radius R_b (thick dashed line), the forward shock velocity $\dot{R}_f$ (thin solid line), the backward shock velocity $\dot{R}_b$ (thin dashed line) and the magnetic field strength (thin dotted line). The ratio of CR energy and energy of supernova explosion E_{cr}/E_{SN} (dotted line) is also shown.

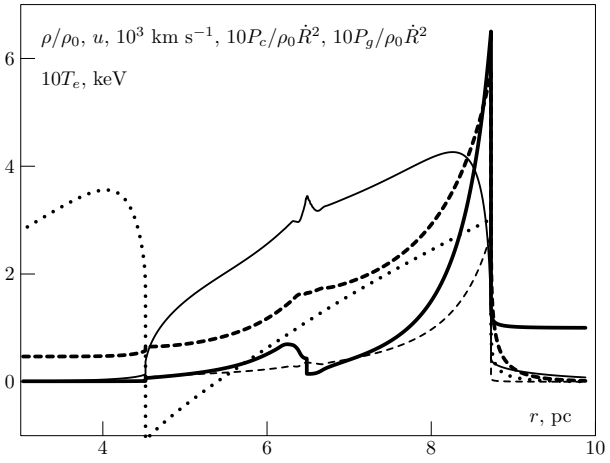

Fig. 2: Radial dependencies of the gas density (thick solid line), the gas velocity (dotted line), CR pressure (thick dashed line), the gas pressure (dashed line) and the electron temperature (thin solid line) at $t = 1050$ yr. At this moment of time the forward shock velocity is 3540 km s^{-1}, its radius is 8.7 pc, the magnetic field strength downstream of the forward shock is 146 μG.

isotropic magnetic field can be considered as a large-scale magnetic field for lower energy particles which are concentrated in the narrow region upstream of the shock. Streaming instability of these particles produces MHD waves propagating in the direction opposite to the CR gradient. This gradient is negative upstream of the forward shock and MHD waves propagate in the positive direction. The situation changes downstream of the forward shock where CR gradient is as a rule positive and MHD waves propagate in the negative direction. This effect is mostly pronounced downstream of the forward shock of SNR because the magnetic field is additionally amplified by the shock compression and the Alfvén velocity $V_A = B/\sqrt{4\pi\rho}$ may be comparable with the gas velocity in the shock frame $u' = \dot{R}_f - u(R_f - 0, t)$. As for CR diffusion coefficient, it is probably close to the Bohm value $D_B = pvc/3qB$, where q is the electric charge of particles.

We apply a finite-difference method to solve Eqs (1-4) numerically upstream and downstream of the forward and backward shock. Auto-model variables $\xi_1 = r/R_f(t)$ and $\xi_4 = r/R_b(t)$ are used instead of radius r upstream of the forward shock at $r > R_f$ and upstream of the backward shock at $r < R_b$ respectively. The gases compressed at forward and backward shocks are separated by a contact discontinuity at $r = R_c$ that is situated between the shocks. We use variables $\xi_2 = (r - R_c)/(R_f - R_c)$ and $\xi_3 = (r - R_c)/(R_c - R_b)$ instead of r between the shocks downstream of the forward and backward shocks respectively.

A non-uniform numerical grid upstream of the shocks at $r > R_f$ and $r < R_b$ allows to resolve small scales of hydrodynamical quantities appearing due to the pressure gradient of low-energy CRs. Eq. (4) for CRs was solved using an implicit finite-difference scheme. An explicit conservative TVD scheme [16] for hydrodynamical equations (1-3) and uniform spatial grid were used between the shocks. These equations are solved in the upstream regions using an explicit finite-difference scheme.

We shall assume that the coordinate dependencies of the magnetic field and the gas density coincide upstream and downstream of the forward shock:

$$B(r) = \sqrt{4\pi\rho_0}\frac{\dot{R}_f\rho}{M_A\rho_0},\ r > R_c. \qquad (5)$$

Here ρ_0 is the gas density of the circumstellar medium. The parameter M_A determines the value of the amplified magnetic field strength. The magnetic energy is about 3.5 percent of the dynamical pressure $\rho_0\dot{R}^2$ according to estimates from the width of X-ray filaments in young SNRs [18]. This number and characteristic compression ratio of a modified SNR shock $\sigma = 6$ correspond to $M_A \approx 23$. Since the plasma density ρ decreases towards the contact discontinuity downstream of the forward shock, the same is true for the magnetic field strength according to Eq. (5). This seems reasonable because of a possible magnetic dissipation in this region.

Situation is different downstream of the backward shock at $R_b < r < R_c$. The plasma flow is as a rule strongly influenced by the Rayleigh-Taylor instability that occurs in the vicinity of the contact discontinuity and results in the generation of MHD turbulence in this region. We shall assume that the magnetic field does not depend on radius downstream of the backward shock while the dependence in the upstream region is described by the equation similar to Eq. (5):

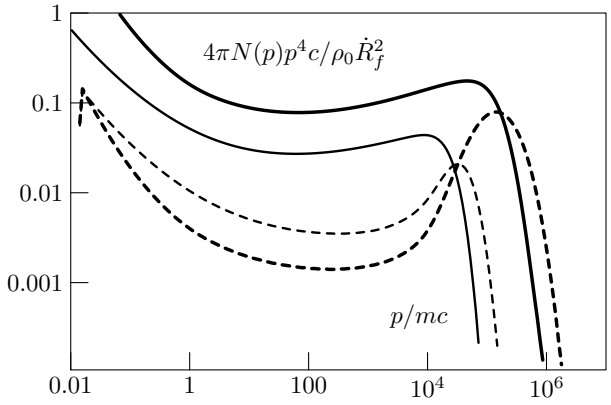

Fig. 3: Spectra of accelerated protons (thick lines) and electrons (multiplied on 5000, thin lines) at $t = 1050$ yr. Spectra at the forward shock (solid lines) and at the backward shock (dashed lines) are shown.

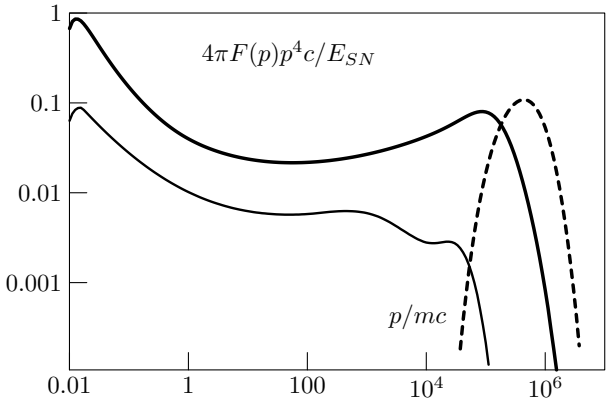

Fig. 4: Spatially integrated spectra of accelerated protons (solid line) and electrons (multiplied on 5000, thin solid line) at $t = 1050$ yr. Spectrum of run-away particles which have left the remnant is also shown (dashed line).

$$B(r) = \sqrt{4\pi\rho_m}\frac{|\dot{R}_f - u(r_m)|}{M_A}\begin{cases} 1, \ r < r_m, \\ \rho/\rho_m, \\ r_m < r < R_b, \\ \rho(R_b+0)/\rho_m, \\ R_b < r < R_c \end{cases} \tag{6}$$

Here $r_m < R_b$ is the radius where the ejecta density has a minimum and equals ρ_m. This radius r_m is generally close to the backward shock radius R_b and is equal to it if the backward shock is not modified by the cosmic ray pressure.

CR advective velocity may differ from the gas velocity on the value of the radial component of the Alfvén velocity V_{Ar} calculated in the isotropic random magnetic field: $w = u + \xi_A V_{Ar}$. Here the factor ξ_A describes the possible deviation of the cosmic ray drift velocity from the gas velocity. Using Eq. (5) we obtain

$$w = u + \xi_A \frac{\dot{R}_f}{M_A}\sqrt{\frac{\rho}{3\rho_0}}, \ r > R_c \tag{7}$$

The similar expression for the cosmic ray drift velocity is used upstream of the backward shock at $r < R_b$. We shall use values $\xi_A = 1$ and $\xi_A = -1$ upstream of the forward and backward shocks respectively, where Alfvén waves are generated by the cosmic ray streaming instability and propagate in the corresponding directions. The damping of these waves heats the gas upstream the shocks and limits the total compression ratios by a number close to 6. The situation is less clear in the downstream region and we shall consider cases $\xi_A = 0$ and $\xi_A = -1$ downstream of the forward shock at $R_c < r < R_f$. In the downstream region of the backward shock we put $w = u$.

We shall use the Bohm energy dependence of CR diffusion coefficient $D = \eta_B D_B$ calculated with the magnetic field strength (5) and (6). The parameter η_B describes the possible deviations of diffusion coefficient from the Bohm value $D_B = vpc/3qB$. Since the highest energy particles are scattered by small-scale magnetic fields, their diffusion is faster than the Bohm diffusion [20]. The same is true for smaller energy particles because they can be resonantly scattered only by a fraction of the magnetic spectrum. We shall use the value $\eta_B = 2$ throughout the paper.

In real situation the level of MHD turbulence drops with distance upstream of the shock and diffusion may be even faster there. The characteristic diffusive scale of highest energy particles is about 1/20 of the shock radius [20] and is determined by the generation and transport of MHD turbulence in the upstream region (see also Vladimirov et al. [17], Amato & Blasi [1]). Since this process is not modelled here, we simply multiply the CR diffusion coefficient D on the additional factor $\exp(20(\xi_1 - 1))$ upstream of the forward shock and on the similar factor $\exp(20(1 - \xi_4))$ upstream of the backward shock.

It is believed that the supernova ejecta has some velocity distribution P(V) just after supernova explosion (e.g. Chevalier [8])

$$P(V) = \frac{3(k-3)}{4\pi k}\begin{cases} 1, \ V < V_{ej} \\ (V/V_{ej})^{-k}, \ V > V_{ej}. \end{cases} \tag{8}$$

Here the index k characterizes the steep power-low part of this distribution. The radial distribution of ejecta density is described by the same expression with $V = r/t$. The characteristic ejecta velocity V_{ej} can be expressed in terms of energy of supernova explosion E_{SN} and ejecta mass M_{ej} as

$$V_{ej} = \left(\frac{10(k-5)E_{SN}}{3(k-3)M_{ej}}\right)^{1/2} \tag{9}$$

Figures (1)-(4) illustrate the numerical results that are obtained for the SNR shock propagating in the medium with hydrogen number density $n_H = 0.072$ cm^{-3} and temperature $T = 10^4$ K. The number density of helium nuclei $0.1n_H$ was assumed. We use the

ejecta mass $M_{ej} = 0.67 M_\odot$, the energy of explosion $E_{SN} = 2.0 \cdot 10^{51}$ erg and the parameter of ejecta velocity distribution $k = 7$. The value $\xi_A = 0$ was used in the downstream region. These parameters correspond to the hadronic scenario of the origin of gamma-rays in the supernova remnant RX J1713.7-3946 (see the companion paper [22] in these Proceedings).

The initial forward shock velocity is $V_0 = 6 \cdot 10^4$ km s^{-1}. The injection efficiency is taken to be independent on time $\eta_b = \eta_f = 0.01$, and the injection momenta $p_f = 2m(\dot{R}_f - u(R+0,t))$, $p_b = 2m(u(R_b-0,t) - \dot{R}_b)$. This high injection efficiency results in the significant shock modification already at early stages of SNR expansion. This is in agreement with the radio-observations of young extragalactic SNRs [9] and with the modeling of collisionless shocks [19]. Since an electron to proton ratio K_{ep} is significantly lower in comparison with an observable Galactic ratio 0.01 at 10 GeV in hadronic models, the electron injection was taken inversely proportional to the square of the shock velocity. Then the electron to proton ratio $K_{ep} \sim 10^{-4}$ for a characteristic shock velocity 3000 km s^{-1} of young SNRs corresponds to $K_{ep} \sim 10^{-2}$ in the old SNRs with characteristic shock velocity 300 km s^{-1}. The old SNRs probably produce the main part of galactic GeV electrons.

The dependencies on time of the shock radii R_f and R_b, the forward and backward shock velocities $V_f = \dot{R}_f$ and $V_b = \dot{R}_b$, CR energy E_{cr}/E_{SN} and the magnetic field strength B_f just downstream the forward shock are shown in Fig.1. The calculations were performed until the moment of time $t = 1050$ yr, when the value of the forward shock velocity drops down to $\dot{R}_f = 3.54 \cdot 10^3$ km s^{-1} and the forward shock radius $R_f = 8.7$ pc at the assumed distance 1 kpc corresponds to the angular radius $30'$ of the remnant RX J1713.7-3946.

At early times of SNR evolution the distance between backward and forward shocks is only 10% of the remnant radius. This is less than 23% thickness for automodel Chevalier-Nadezhin solution with $k = 7$ [7] and should be attributed to a strong modification of both shocks by CR pressure. The backward shock is strongly decelerated only when the forward shock sweeps the gas mass comparable with the ejecta mass at $t > 100$ yr and when the transition to the Sedov phase begins. It is important that the observable ratio $R_b/R_f = 0.5$ is achieved at the Sedov phase when the forward shock velocity is close to one third of the characteristic ejecta velocity V_{ej}. Since SNR RX J1713.7-3946 produces a lot of hard nonthermal X-rays, the forward shock velocity is hardly lower than $3 \cdot 10^3$ km s^{-1} now. Therefore the characteristic ejecta velocity is not smaller than 10^4 km s^{-1} for this supernova. Such high velocities may be attributed to Ib/c and IIb core collapse supernovae with low ejecta masses, but not to the most frequent core collapse IIP supernovae with characteristic ejecta velocities $3 \cdot 10^3 - 4 \cdot 10^3$ km s^{-1} and high ejecta masses.

Radial dependencies of physical quantities at $t = 1050$ yr are shown in Fig.2. The contact discontinuity between the ejecta and the interstellar gas is at $r = R_c = 6.5$ pc. The backward shock in the ejecta is situated at $r = R_b = 4.5$ pc. At the Sedov stage the backward shock moves in the negative direction and reach the center at two thousand years after the supernova explosion.

It is desirable to know the electron temperature for calculation of thermal X-ray emission. Since thermal electrons are not in temperature equilibrium with ions in young supernova remnants, we take into account a minimum available electron heating that is the heating by Coulomb collisions [15]. The corresponding temperature is also shown in Fig.2.

Spectra of accelerated protons and electrons are shown in Fig.3. At this moment of time the maximum energy of protons accelerated in this SNR is about 200 TeV, while higher energy particles have already left the remnant. The spectra at the backward shock show large bumps just before cut-offs. This is because the backward shock moves in the rarefied medium of the ejecta now and the amount of freshly injected small energy particles is relatively low while many high energy particles accelerated earlier have not left the backward shock yet.

Spatially integrated proton and electron spectra for $t = 1050$ yr are shown in Fig.4. We also show the spectrum of run-away particles. These particles have already left the simulation domain through an absorbing boundary at $r = 2R_f$. The sum of the proton spectra shown should be considered as a cosmic ray spectrum produced in this SNR during 1050 years after SN explosion. The cosmic ray protons have the maximum energy close to 1 PeV for this SNR.

REFERENCES

[1] Amato, E., & Blasi, P., 2006, MNRAS, 371, 1251
[2] Axford, W.I., Leer, E., Skadron, G., 1977, Proc. 15th Int. Cosmic Ray Conf., Plovdiv, 90, 937
[3] Bell, A.R., 1978, MNRAS, 182, 147
[4] Bell, A.R., 2004, MNRAS, 353, 550
[5] Berezhko, E.G., Elshin, V.K., Ksenofontov, L.T., 1994, Astropart. Phys. 2, 215
[6] Blandford, R.D., & Ostriker, J.P. 1978, ApJ, 221, L29
[7] Chevalier, R., 1982, ApJ, 258, 790
[8] Chevalier, R., 1982, ApJ, 259, 302
[9] Chevalier, R. 2006, ApJ 651, 381
[10] Jun, B., & Norman, M.L., 1996, ApJ 465, 800
[11] Kang, H., Jones, T.W., 2006, Astropart. Phys. 25, 246
[12] Krymsky, G.F. 1977, Soviet Physics-Doklady, 22, 327
[13] Lagage, P.O., & Cesarsky, C.J., 1983, A&A, 118, 223
[14] Malkov, M.A., & Drury, L.O'C, 2001, Reports on Progress in Physics, 64, 429
[15] Spitzer, L. 1968, Diffuse matter in space (New York: Intersience)
[16] Trac, H., Pen, U. 2003, Publ. Astron. Soc. Pacific 115, 303
[17] Vladimirov, A., Ellison, D.C., & Bykov, A., 2006, ApJ, 652, 1246
[18] Völk, H.J., Berezhko, E.G., & Ksenofontov, L.T., 2005, A&A, 433, 229
[19] Zirakashvili, V.N. 2007, A&A 466, 1
[20] Zirakashvili, V.N., Ptuskin, V.S., 2008, ApJ 678, 939
[21] Zirakashvili, V.N., & Ptuskin, V.S. in preparation
[22] Zirakashvili, V.N., & Aharonian, F. these Proceedings